Proceedings of the 26th International Conference on
Port and Ocean Engineering under Arctic Conditions
June 14-18, 2021, Moscow, Russia

Scale-model ridges and interaction with narrow structures, Part 4 Global loads and failure mechanisms

Zongyu Jiang[1,2], Jaakko Heinonen[3], Maria Tikanmäki[3], Eeva Mikkola[3], Ilkka Perälä[3], Aleksey Shestov[4], Knut V. Høyland[1], Evgenii Salganik[1], Marnix van den Berg[1], Hongtao Li[1], Åse Ervik[5], Otto Puolakka[2]
[1] NTNU, Trondheim, Norway
[2] Aalto University, Espoo, Finland
[3] VTT, Espoo, Finland
[4] UNIS, Longyearbyen, Norway
[5] Multiconsult, Tromsø, Norway

ABSTRACT

An experimental campaign was carried out in the Aalto ice basin to investigate sea ice ridge interaction with bottom-fixed structures. The campaign covered three different ice sheets and ridges. Punch tests, flexural strength test and compressive strength test were carried out on the model ice. Two different structures were tested, one with cylindrical and one with conical waterline (cone angle 75°). A geometric scale-factor of 15 was applied between the model and prototype. The model was pulled through the ridges while measuring the loads. A monitoring system with six cameras was installed to observe the deformation pattern of ice. Two of these cameras were installed above the sea surface and four of them were installed underwater. The failure mode of ridge keel was observed by using underwater cameras, and observations showed that the breaking of keel had a shrinkage-expansion pattern before all freeze bond in front of the structure was broken by the structure. For the consolidated ridge, the cone part of the structure could reduce the ice loads induced by the consolidated layer, but the cone did not effectively influence the loads induced by rubble due to its short length. For the unconsolidated ridge, the cone could reduce the ice loads due to weak confinement of the contacting rubble near water line.

KEY WORDS: Model test; Ice ridge; Ice loads; Keel failure observation; Vertical and conical structures

INTRODUCTION

The activities of human being are increasingly frequent in the Arctic area. More and more offshore, coastal structures and ships are deployed in the cold region where human being seldom visited in the past. In addition, more structures are being deployed in the cold region with many human being activities too. |For example, offshore wind turbines are being built in the Baltic. The marine structures inevitably face the threat of sea ice, which induces loads threatening the structures. The prediction of ice loads has huge uncertainty due to the complicated micro-structure of sea ice and its various formation, such as the ice ridge. The ice ridge is inhomogeneous, and its strength depends on the degree of consolidation (Blanchet, 1998 and Høyland, 2002). An ice ridge has a sail and a keel, and the keel is often separated into an upper refrozen consolidated layer and a lower unconsolidated part. The consolidated layer is thicker than the level ice but has similar mechanical properties. The rubble consists of loosely bonded ice blocks and, consequently, is much weaker than the consolidated layer. When a ridge interacts with a structure, several different processes and failure mechanisms take place. Therefore, an important research question is to quantify these different processes and how they depend on ridge consolidation and structural shape.

A common approach to determine ridge loads is to separately deal with the consolidated layer and keel (Croasdale and Allyn, 2018). The consolidated layer is considered as thick level ice, and analytical models for ice action depend on structural geometry (ISO19906, 2019). The action from the ice rubble is often determined through models for "soil mechanics" (Dolgopolov et al., 1975; Croasdale, 1980; Kärnä et al., 2001).

This paper presents results about ice ridge loads from a model-scale experiments conducted in 2019 in Aalto ice tank, an overview of the experiment was given in Shestov et al. (2020). Two different structures were used: 1) cylindrical structure, with a shell perpendicular to the level ice; 2) conical structure, with a shell intersecting the level ice at an angle of 75 degree to the level ice. With these two types of structures, a comparative study was conducted to investigate the ice loads on the vertical structure and the sloped structure. Six cameras were installed above and under water to observe the process of ice ridge breaking and rubble accumulation around the structure. The most interesting observation is that the rubble loads are more closely connected to the maximum horizontal extension of rubble pushed by the structure rather than the depth of accumulation.

EXPERIMENTAL SET-UP AND PROCEDURES

The model tests were conducted in the Aalto Ice Tank of Aalto University. This section describes the testing facilities, model ice, model and prototype structure, model-scale, testing procedure etc.

Experiment facilities

The dimension of Aalto Ice Tank is 40 m long, 40 m wide and 2.8 m deep. A towing carriage is installed above the ice basin to carry testing subjects to run in longitudinal and transversal directions while performing the tests. A set of cooling machinery and heat exchangers are used to change the air temperature of the Ice tank in order to grow and temper the model ice in the ice basin.

The global ice loads were measured by a six DOF load cell connected to the structure by a flange and pins. The force and moment sensitivities have a maximum deviation of 5%. The origin of the sensor coordinates was at the vertical axial line of the model. The vertical distance was 0.094 m between the origin of the sensor coordinates and the top of the conical part of the model.

Six cameras were attached to the model to monitor the behavior of structure and ice, especially to record the failure modes of ice and the rubble accumulation. Two cameras were above the water surface, and four cameras were installed underwater, as shown in Fig. 1.

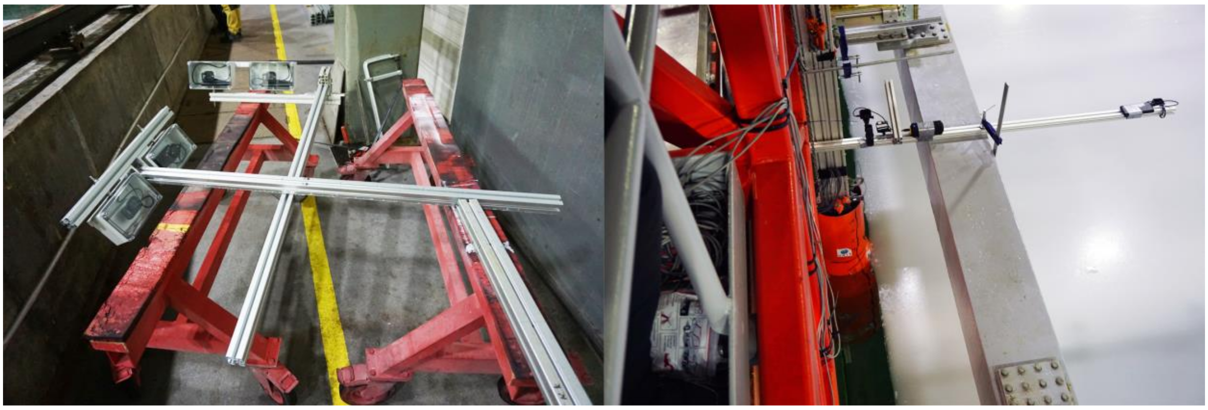

Figure 1. Installed above- and under-water cameras

Model ice production

The procedure of making and consolidating the ridges is given in Shestov et al. (2020). The maximum depth of keel was approximate 0.4 m. The width of ridge was generally 4 m and started from the side close to the structure.

Model structure and test matrix

The model is 0.54 m in diameter and 1.3 m in length. In order to compare the ice loads on cylindrical structure and conical structure, a approximately 0.4 m long conical part was added to the model, with a slope angle of 75 degree. The main dimension of the model is shown in Shestov et al. (2020).

Table 1. Overview of testing, structure, consolidation and properties.

Ice sheet #	Test #	Consolidated	Structure waterline	Testing in Level ice before	Testing in Ridge	Testing in Level ice after	Level ice flexural strength (MPa)
1	1	Y	Vertical	N	Y	N	73
2	2	N	Vertical	Y	Y	Y	60
	3		Vertical	N	N	N	
	5	Y	Sloping	N	Y	Y	235
	6	Y	Sloping	Y	Y	Y	235
3	7	N	Sloping	Y	Y	Y	51
	8	N	Sloping	Y	Y	Y	51
	9	Y	Sloping	Y	Y	Y	78
	10	Y	Vertical	N	Y	N	78

Table1 shows the test matrix, which consists of two different structural shapes (vertical and sloping), consolidated (tests 1, 5, 6, 9 and 10) and unconsolidated ridges (tests 2, 7 and 8). The experiment also run the structures through the level ice whenever possible.

TEST RESULTS, MAIN OBSERVATIONS AND DISCUSSION

This study focuses on the ice loads along the towing direction (x-direction), which was perpendicular to the ridge, because the magnitude of forces in x-direction is much larger than those in lateral and vertical directions. Consequently, the X axis points in the reverse direction of motion of the model. Therefore, only ice loads in x-direction are presented for analysis and discussion.

Note that the bottom of conical part of model was approximately 0.2 m beneath the water line so the sloping wall could only influence the breaking of level ice or consolidated layer. The structure fully cut through the ridges in six of the eight tests. At Test 1 and Test 10, the structure could not fully cut through the ridges due to extremely high ice loads.

Load-time history curve and envelope

Figure 2 illustrates the load-time history curve of ice loads induced by the ice ridge. The left vertical axis gives the magnitude of ice loads, and the horizontal axis is the distance that the model penetrated into the ridge. As described above, Test 1 and 10 could not run through level ice, because the level ice was too strong. The spikes, towards the end of these tests, appeared when the structure entered the ice behind the ridges. The other curves also show the level ice loads after 4 m penetration distance. The right vertical axis indicates the magnitude of accumulated rubble depth and maximum horizontal extension in front of the model structure.

When the model penetrated through the ridge, the ice loads were induced by breaking the consolidated layer and deforming the rubble. The high-frequency oscillation of the curve was attributed to the breaking of consolidated layer. Thus, the upper envelope and lower envelope of curves could be used to represent the total ice loads and ice loads induced by the rubble, respectively. One example is shown in Fig. 3. The difference between the upper and lower envelopes could be considered as the ice loads induced by the consolidated layer. Please note that the lower envelope might be an underestimation of the rubble loads due to the vibration of the structure. Consequently, difference between the upper and lower envelopes might be an overestimation of the consolidated layer load. Nevertheless, the evolution of rubble load magnitude could be represented by the lower envelope. The lower envelopes are used to discuss the connection between the rubble loads and the rubble accumulation.

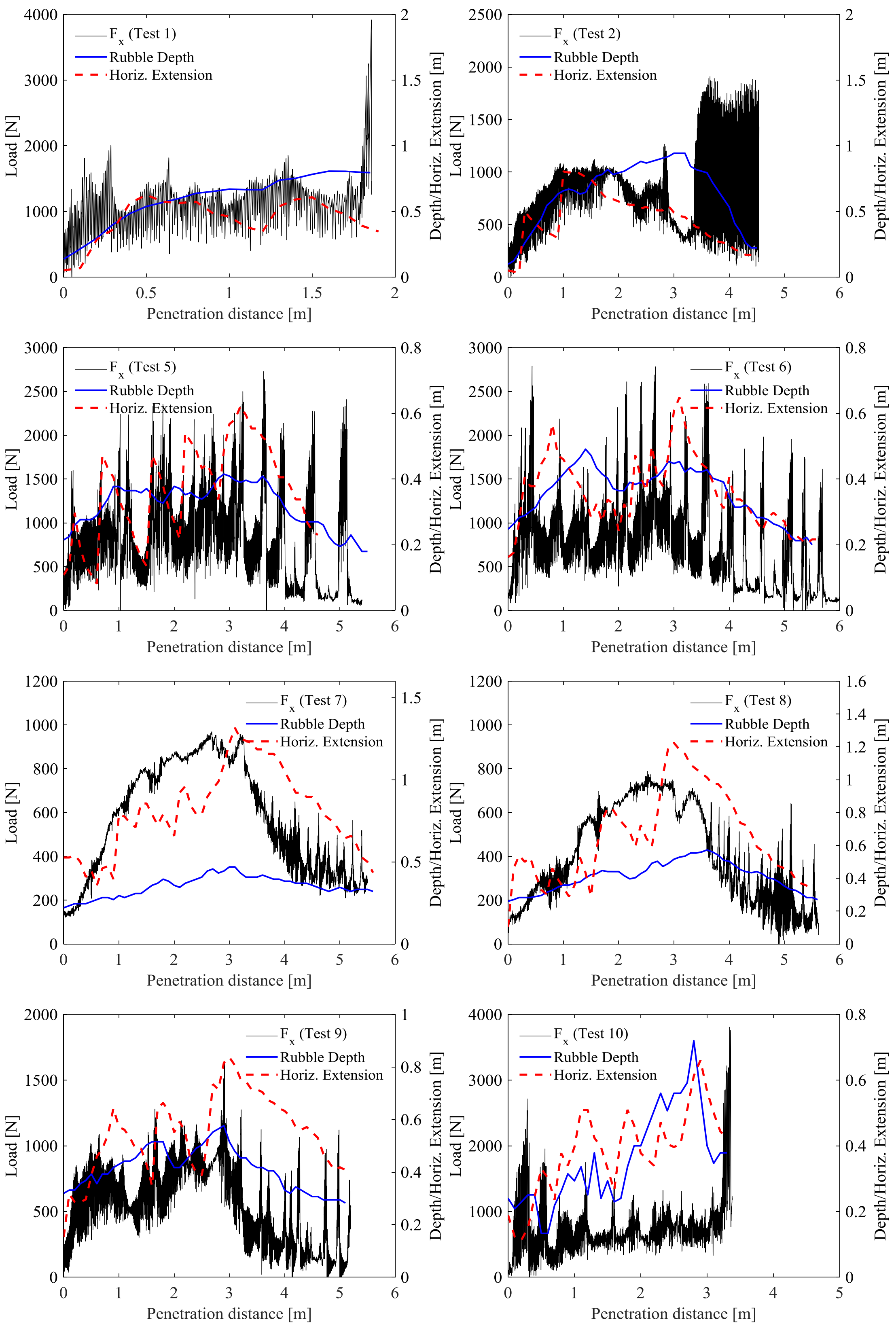

Figure 2. History curve of ridge loads, keel profile, rubble depth and rubble horizontal extension

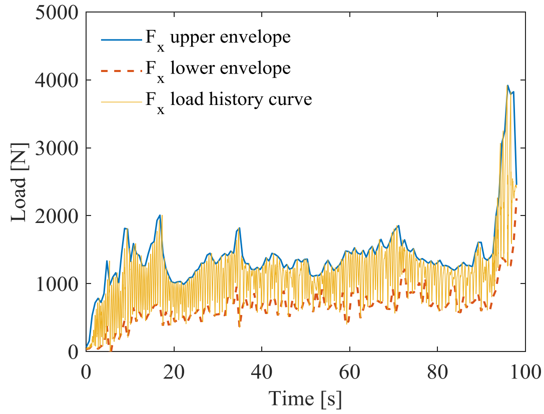

Figure 3. Envelopes of ice loads in X direction at Test 1 (Vertical Structure)

Rubble accumulation

When the model cut through the ridge, the rubble accumulation was observed in front of the model. The underwater videos showed that the longitudinal central section of the rubble accumulation could roughly be estimated as a triangle (Fig. 4). Two parameters are employed to represent the variation of rubble volume accumulated in front of the model: maximum depth of the rubble accumulation and the maximum horizontal extension of rubble moved by the model (Fig. 4).

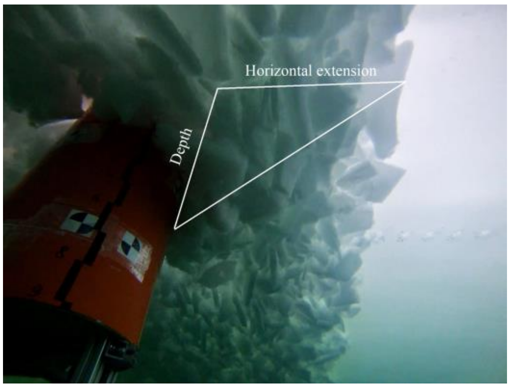

Figure 4. Rubble accumulation in front of the model at Test 9

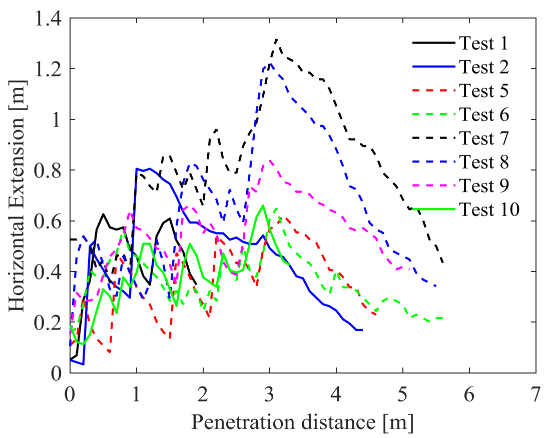

Figure 5. Horizontal moving rubble extension in front of the structure (Vertical Structure: Test 1, 2 & 10; Slope Structure: Test 5~9)

Figure 5 shows the maximum horizontal extension of moving rubble against the penetration distance of the structure. In most cases, the largest peaks were located at roughly 3 m penetration distance. The total width of ridge is 4 m, so the extension of moving rubble reached its highest magnitude at around 75% ice ridge width. However, it should note that it is not clear how this value was connected to the ice ridge width and/or the diameter of the column type structure. One exception is Test 2. At Test 2, the highest extension of moving rubble located at around 1.2 m penetration distance. At Test 1 and 10, the structure did not fully penetrate the ice ridge so the data did not show the highest extension.

At the ascending stage before the summit, the curves rose up with a zigzag pattern. When the structure contacted the keel, the contacting force firstly broke the freeze bond between rubble which were close to the structure. This part of rubble was pushed to move forward. The moving rubble were squeezed by the structure and immobile rubble. At first, the pushing force was less than the strength of freeze bond at the boundary of moving rubble extension. Therefore, the rubble beyond the boundary did not move. As a result, the horizontal extension of moving rubble kept shrinking due to the advance of model. This was the situation on the left side of a tooth in the moving rubble horizontal extension curve. The structure continuously pushed the rubble to reduce the porosity between rubble. The contacting force continuously increased along with the increase of squeezing level until the contacting force became large enough to break the freeze bond beyond the boundary. At this time, the horizontal extension of moving rubble turned into expansion and another round started. Figure 5 also shows that zigzag patten was more apparent if the freeze bond was stronger. Figure 6 presents an example of the whole procedure of horizontal extension shrinkage and expansion. The straight lines point out the boundaries of moving rubble at various penetration distances.

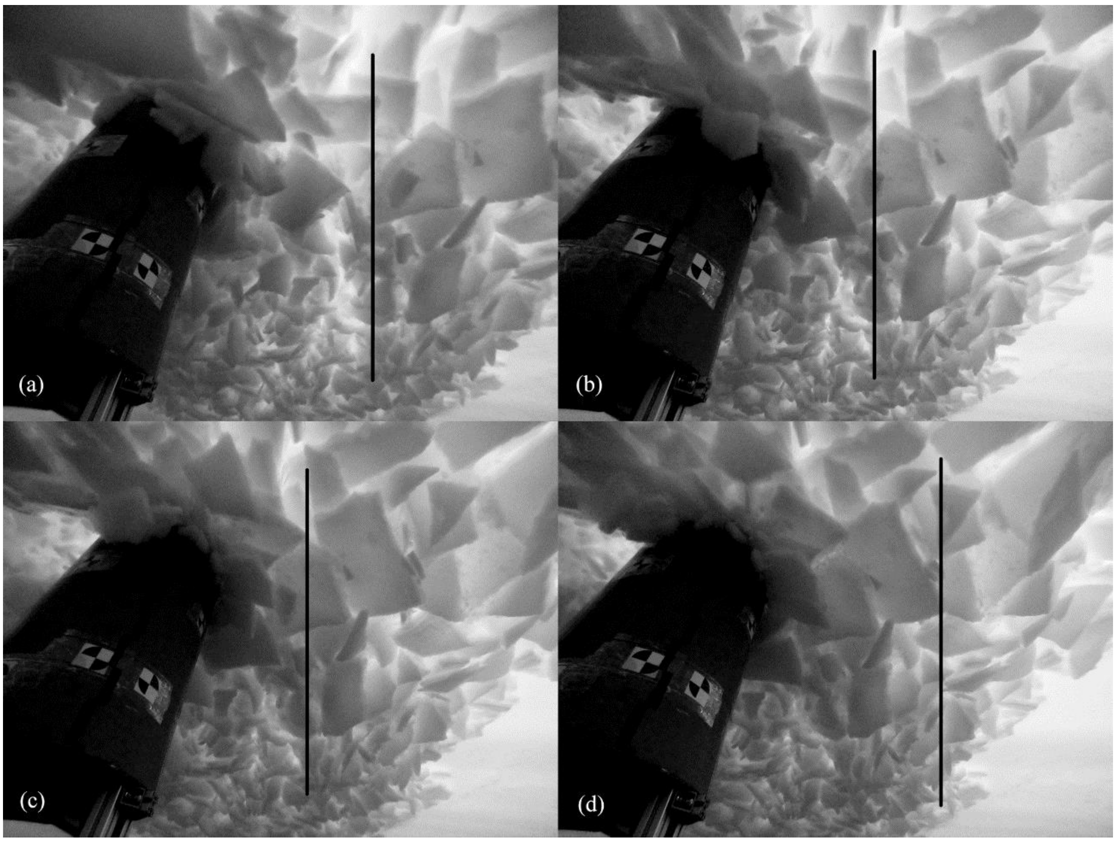

Figure 6. Shrinkage and expansion of maximum moving rubble horizontal extension at Test 5 (Slope Structure), penetration distance is 1.6 m (a), 1.8 m (b), 2.1 m (c) and 2.2 m (d).

When the horizontal extension of moving rubble reached the opposite boundary of the keel, its magnitude also rose up to the maximum in most cases. After this point, the magnitude of horizontal extension continuously decreased due to the clearing of rubble. At the descending stage, all freeze bonds between rubble were broken and the structure only needed to push the rubble forward, so the curves were smoother than those at the ascending stage.

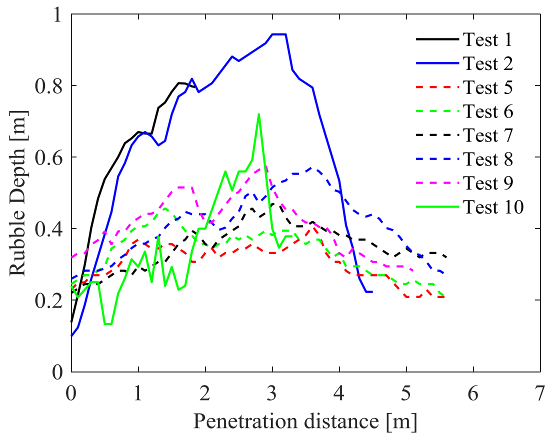

Figure 7. Maximum depth of rubble accumulation in front of the structure (Vertical Structure: Test 1, 2 & 10; Slope Structure: Test 5~9)

Figure 7 shows the maximum depth of rubble accumulating in front of the structure. The summits of most cases located at the second half of the keel, approximately after 3 m penetration distance. However, the curve of Test 6 had a summit at around 1.5 m penetration distance. Test 1 and 10 did not penetrate the whole keel so its summit location could not be observed during the test. The curves rose up with severer fluctuation on the left of the summits. It was attributed to combining effect of rubble accumulation and clearing. Generally, the accumulation dominated the variation of rubble depth, but the clearing might exceed the accumulation at some specific time points. Consequently, the rubble depth decreased and resulted in a dent at the curve of rubble depth. After the summit, the rubble depth was only influenced by the rubble clearing so the curves were smoother.

As shown in Fig. 4, the longitudinal central section of rubble accumulation was triangle in geometry according to the observation. Therefore, the area of the section is employed to represent the amount of accumulation

$$A = DR/2 \tag{1}$$

where D denotes the rubble depth and R denotes the maximum horizontal extension of rubble. Thus, the area of the section A could reflect the influence of depth and horizontal extension on the rubble loads.

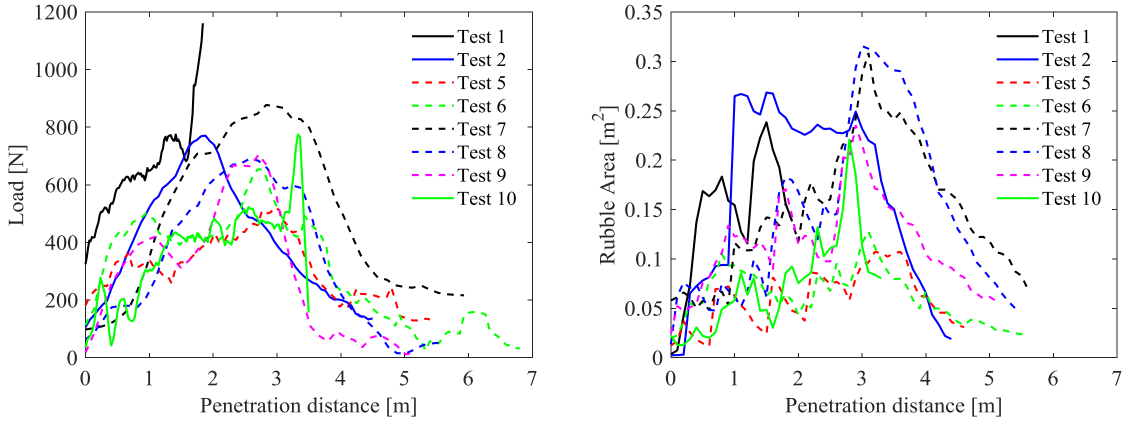

Figure 8. Lower envelop of ridge loads and longitudinal central section area (Vertical Structure: Test 1, 2 & 10; Slope Structure: Test 5~9)

Figure 8 shows the lower envelop of ridge loads and area of section A of Test 1 ~ 10. It was clear that the pattern of load curve fairly matched the trend of section area curve for each case. For example, the summit of two kinds of curves had close location at X axis. Gong et al. (2019) reported a discrete element simulation to predict resistance of a ship in unconsolidated ridges. According to their findings, the deformation force maintains a constant maximum magnitude when the ship bow fully enters the ridge and the deformation force is proportional to the volume of ice rubble moved by the ship. Our observation is consistent with their results. The rubble area curves also showed that the rubble accumulation was larger at the tests with unconsolidated keel. In ice sheet 2, the curve of Test 2 was generally higher than the curves of Test 5 and 6. In ice sheet 3, the curves of Test 7 and 8 were generally higher than the curves of Test 9 and 10. This could be ascribed to the difference of freeze bond strength in different cases. In the ridge with consolidated layer, the freeze bond between rubble was stronger than that of ridge without consolidated layer so the structure could move fewer ice rubble by breaking their freeze bond. As a result, the rubble accumulation was smaller. It should note that the lower envelope underestimated the loads induced by the keel because of the structure's vibration. The underestimation might be larger if the vibration was stronger. Thus, the tests in ridge with consolidated layer were more underestimated than the tests in ridge without consolidated layer. Therefore, the curves could not be applied for comparing the keel loads between different cases.

Components of ice loads

Figure 9 presents the maximum measured ice loads and their components induced by ridge. Please note that this figure does not show the extremely large loads which caused the abortion of Test 1 and 10. It shows that the fluctuation of ice loads induced by the consolidated layer was much larger than the fluctuation of ice loads induced by the rubble. The ice loads induced by the consolidated layer is calculated by subtracting rubble loads from total loads. Test 2, 7 and 8 were conducted before consolidation, hence small consolidated layer loads were expected. The measurements from Test 7 and 8 were in compliance with the expectation. However, the measurement from Test 2 shows that the maximum consolidated layer load was approximately 1000 N and close to the rubble load. This large magnitude could be attributed to the confinement of the rubble contacting the model. At Test 2, the model had cylindrical water line and it pushed the contacting rubble to the surrounding rubble. As a result, the confinement increased the difference between the upper and lower envelope. In contrast, the slopping wall pushed the contacting rubble upwards at Test 7 and 8. Thus, the difference between the upper and lower envelope could be very small. For the ridge with consolidated layer, the measurements at Test 9 and 10 show that the sloping structure could reduce the ice loads induced by the consolidated layer.

The rubble loads did not fluctuate much in maximum magnitude from test to test. This suggested that the structural type and consolidation did not have obvious influence on the rubble loads. As to the structural type, it is easy to understand because the conical part was very short compared to the total length of the model. The conical part only extended to as far as 0.2 m beneath the water line. Thus, it only affected a small upper part of rubble. Furthermore, the upper part of moving rubble is most confined by surrounding rubble. As to the consolidation of ridge, its influence could not be observed from Fig. 9.

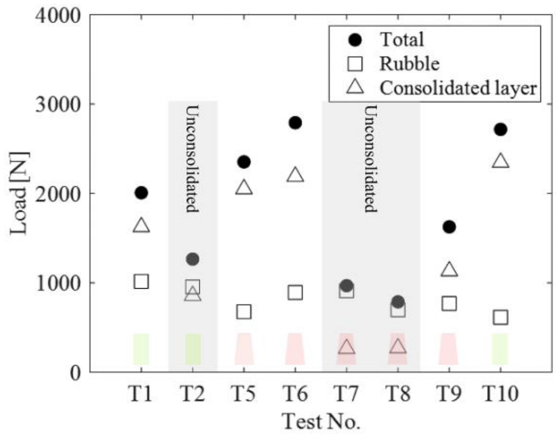

Figure 9. Components of ice loads induced by ridge

CONCLUSIONS

An experiment campaign was conducted in the Aalto Ice Tank to study the ice ridge loads on cylindrical and conical structures. Eight tests were successfully performed by running the model through three ice sheets with an embedded ridge. These three ice sheets had constant thicknesses and various flexural strength. The model, consisting of conical part and cylindrical part, was fixed on the carriage and towed to run through the ice. Eight tests were successfully conducted. At each test, only one part was utilized to investigate the properties of interaction between the ice and vertical/slope structures. The measured ice loads were separated into two components: 1) consolidated layer loads, loads induced by the consolidated layer, and 2) rubble loads, loads induced by the rubble.

Based on the investigation of the ice loads measurements and the breaking process of ridge, the following conclusions could be made:

1) The rubble loads were proportional to the volume of rubble accumulation in front of the model structure.

2) The process of breaking the keel was not smoothly continuous. The process had an obvious pattern of shrinkage and expansion in the horizontal extension of rubble moved by the model. This pattern vanished when the horizontal extension reached the farthest edge of the ridge.

3) The consolidation of ridge and cone at water line did not have obvious influence on the maximum magnitude of rubble loads. The influence of cone was weak because of its short length compared with the whole length of the model.

ACKNOWLEDGEMENTS

The work described in this publication was supported by the European Community's Horizon 2020 Programme through the grant to the budget of the Integrated Infrastructure Initiative HYDRALAB+, Contract no. 654110. The authors would also like to thank the crew in the Aalto ice basin for the hospitality and fixing all practical matters during the long hours of testing.

REFERENCES

Blanchet, D. 1998. Ice loads from first-year ice ridges and rubble fields. *Canadian Journal of Civil Engineering*, 25(2), 206-219.

Croasdale, K.R. 1980. *Ice forces on fixed, rigid structures*. U.S. Army Cold Reg. Res. Eng. Lab., Special Rep. No. 80-26.

Croasdale, K., & Allyn, N., 2018. Ridge Loads on Wind Turbine Structures. *In OTC Arctic Technology Conference*. Offshore Technology Conference.

Dolgopolov, Y., Afanasiev, V., & Panfilov, D. 1975. Effect of hummocked ice on the piers of marine hydraulic structures. *Proceedings of the 3rd IAHR International Symposium on Ice*, Hanover, NH. pp. 463-477.

Gong, H., Polojärvi, A., & Tuhkuri, J. 2019. Discrete element simulation of the resistance of a ship in unconsolidated ridges. *Cold Regions Science and Technology*, 167, 102855.

Høyland K.V., 2002. Consolidation of first-year sea ice ridges. *Journal of Geophysical Research: Oceans*, 107(C6): 15-1-15-16.

International Standards Organization (ISO), 2019. Petroleum and natural gas industries - Arctic offshore structures. ISO 19906:2019.

Kärnä, T., Chae, W. R., & Shkhinek, K., 2001. Global loads due to first-year ice ridges. *In The 16th International Conference on Port and Ocean Engineering under Arctic Conditions (POAC)*, Ottawa, Canada, 627-638.

Shestov, A., Ervik, A., Heinonen J., Perälä, I., Høyland K.V., Salganik E., Li, H., van den Berg, M., Jiang, Z., Puolakka, O., 2020. Scale-model ridges and interaction with narrow structures, Part 1: Overview and scaling. *In Proceedings of the 25th IAHR International Symposium on Ice*. Trondheim, Norway. June 14-18, 2020. International Association for Hydro-Environment Add Engineering and Research (IAHR).